DALTON
FULL PAPER

Supramolecular networks *via* hydrogen bonding and stacking interactions for adenosine 5′-diphosphate. Synthesis and crystal structure of diaqua(2,2′:6′,2″-terpyridine)copper(II) [adenosine 5′-diphosphato(3−)](2,2′:6′,2″-terpyridine)cuprate(II) adenosine 5′-diphosphate(1−) hexadecahydrate and density functional geometry optimization analysis of copper(II)- and zinc(II)-pyrophosphate complexes

Renzo Cini * and Claudia Pifferi

Dipartimento di Scienze e Tecnologie Chimiche e dei Biosistemi, Università di Siena, Pian dei Mantellini 44, I-53100 Siena, Italia. E-mail: cini@cuces.unisi.it

Received 7th October 1998, Accepted 12th January 1999

Single crystal X-ray diffraction showed that crystals of $[Cu(TERPY)(H_2O)_2][Cu(TERPY)(ADP)][H_2ADP]\cdot 16H_2O$ [TERPY = 2,2′:6′:2″-terpyridine; ADP = adenosine 5′-diphosphate(3-)] belong to the triclinic system, space group *P*1 (no. 1) and contain free nucleotide molecules, nucleotide molecules linked to the metal centre of $Cu(TERPY)^{2+}$ units, $[Cu(TERPY)(H_2O)_2]^{2+}$ complexes and free water molecules. The molecules of free nucleotide, $[Cu(TERPY)(ADP)]^-$ and $[Cu(TERPY)(H_2O)_2]^{2+}$ are clustered together and interact *via* the phosphate moieties and the $Cu(H_2O)_2^{2+}$ group. An extensive web of hydrogen bonds holds the three molecules oriented in such a way that the most hydrophobic regions (TERPY) occupy the perimeter of a pocket which contains the pyrophosphate systems. Stacking interactions between the adenine rings and the TERPY ligands stabilize the supramolecular aggregates. Owing to the high content of cocrystallized water molecules the nucleotides have an environment similar to the aqueous phase. The analysis of the Fourier-difference map and of the geometrical parameters of the molecules is consistent with a model in which the free nucleotide molecule is protonated at N(1) and phosphate(β), whereas the copper-bound nucleotide molecule is fully deprotonated as regards the N(1) and phosphate oxygen atoms. The phosphate(β) of the copper-bound nucleotide behaves as a better ligand than phosphate(α) [Cu–O, 1.919(8) and 2.244(10) Å, respectively]. The chelation to the metal of the pyrophosphate moiety causes a lengthening of 0.040(9) Å of the P(β)–OP bond with respect to P(α)–OP. A density functional analysis at the B3LYP/LANL2DZ level was carried out on $P_2O_7^{4-}$, $HP_2O_7^{3-}$, $[Cu(O,O\text{-}PO_4)]^-$, $[Cu\{O(\alpha),O(\beta)\text{-}P_2O_7\}]^{2-}$, $[Zn\{O(\alpha),O(\beta)\text{-}P_2O_7\}]^{2-}$, $[Zn\{O(\alpha),O(\beta)\text{-}HP_2O_7\}(H_2O)(OH)]^{2-}$, $[Cu\{O(\alpha),O(\beta)\text{-}HP_2O_7\}(NH_3)_3]^-$ and $[Zn\{O(\alpha),O(\beta)\text{-}HP_2O_7\}(NH_3)_2]^-\cdot NH_3$. The computational procedure was able to reproduce the overall conformation (bond and torsion angles) of the pyrophosphate group as well as the structure of the co-ordination ring found in the solid state. The computed fully optimized structure for $[Cu\{O(\alpha),O(\beta)\text{-}P_2O_7\}]^{2-}$ has a Cu–O bond distance of 1.837 Å and the co-ordination ring has a boat-envelope conformation, in agreement with the experimental structure found for the metal-bound nucleotide molecule.

The structural characterization *via* diffraction techniques of metal-nucleoside polyphosphate complexes is a difficult task because of the problems encountered in growing suitable single crystals. In spite of the significant improvements in experimental devices for data collection, like high power sources and reliable fast detecting tools, the number of accurate crystal structure analyses for metal–nucleoside polyphosphates so far reported is quite small.[1a] The presence of many complex species in the mother-solution, of differently protonated forms, of conformation equilibria, and the occurrence of hydrolytic processes on the phosphate chain catalysed by the metal ions are some of the causes of frustration. The enormous scientific interest about nucleoside 5′-diphosphate and -triphosphate arises because the most important bioenergetic processes involve ATP (adenosine 5′-triphosphate), ADP, AMP (adenosine 5′-monophosphate), phosphate and pyrophosphate (or diphosphate).[1b,c] A general feature of enzymes which catalyse the hydrolysis of phosphoanhydride bonds is the requirement of divalent metal ions for activation.[1d] These enzymes recognize divalent cation (usually magnesium)–nucleotide complexes as substrates, rather than free nucleotide molecules.[1e]

The investigation of metal–nucleoside, -nucleotide linkages is also of importance to understand metal–nucleic acid interactions and the biological mechanism of certain metal based drugs.[1f–l] Moreover, nucleotide and nucleoside analogues are investigated as drugs, mostly for their antiviral activities.[1m,n]

The knowledge of accurate geometrical parameters from diffraction studies in the solid state of nucleoside 5′-diphosphate and -triphosphate molecules as well as those of the relevant metal complexes is very important for understanding the co-ordinating ability, hydrogen bond formation and base pairing schemes, and the conformation of flexible moieties such as ribose and phosphates. What can be learnt from such studies throws light on many biochemical processes and helps in interpreting the Fourier maps calculated from diffraction data of crystals containing enzyme–nucleotide adducts. To cite a few examples, in the work by Löwe and Amos[2] on the structure of a 1:1 adduct between FtsZ protein (a GTPase in eubacteria; after filamenting temperature-sensitive mutant Z genes) and GDP (guanosine 5′-diphosphate), by Davies *et al.*[3] on the structure of a 1:1 adduct between 3-phosphoglycerate kinase from a procaryotic cell and ADP, and by Janin and co-workers[4] on

the structure of a nucleoside diphosphate kinase–ADP-Mg^{2+} complex, the authors stress how the conformation of the phosphate chain and ribose, the method of linking of the nucleotide to metal ions, the hydrogen-bond formation to the base, sugar and phosphate moieties are the basis of molecular recognition, self-assembly and catalytic activity of the protein also in the particular cases of nucleoside diphosphates as substrates. The concepts of self-assembly, molecular recognition and supramolecular chemistry[5,6] are strictly related and have been noted and emphasized in a growing number of scientific reports.[7,8] Metal–ligand co-ordination, electrostatic forces, hydrogen bonds, stacking interactions, cation π system[9] and (R)H–π system interactions,[10] and torsional equilibria control the self-assembly processes. In biological systems all these components are interconnected and chemists have only a very poor understanding of the ways through which they relate to one another to give self-assembly and dynamic effects. In all the cases of biological importance water molecules and protonation/deprotonation processes play an important role for influencing the conformation of biomolecules and the method of assembling molecular aggregates. In turn the success in growing crystals depends in general on the process through which molecular subunits spontaneously aggregate (i.e. chemical self-assembly).

Efforts devoted to understanding metal–nucleoside and –nucleotide co-ordination have continued in this laboratory[11–14] and attention was recently focused on three aspects: (1) the choice of a second ligand which can occupy up to three co-ordination sites so reducing the number of donors from the nucleotide ligand;[14] (2) the supramolecular structures organized in highly hydrated crystals; (3) the ability of accessible (also for an inorganic chemistry laboratory) theoretical approaches to simulate the covalent metal–ligand systems and the non-covalent complex–ligand interactions. Here we report on the preparation and structural characterization of highly hydrated single crystals containing adenosine 5′-diphosphate and copper(II) ions with the stoichiometry $[Cu(H_2O)_2(TERPY)]$-$[Cu(TERPY)(ADP)]$ $[H_2ADP]\cdot 16H_2O$, and on the density functional geometry optimization of model systems. The existence of supramolecular aggregates of complex molecules, H_2ADP^- molecules and water molecules is deeply analysed and discussed.

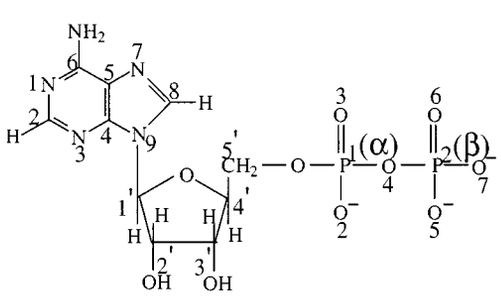

Experimental

Materials

Di(cyclohexylammonium)adenosine 5′-diphosphate 2.5 hydrate $[MCHA]_2[HADP]$ was purchased from Sigma, 2,2′ : 6′,2″-terpyridine from Fluka, copper(II) sulfate pentahydrate, analytical grade, from Carlo Erba and 96% EtOH from Merck. All the chemicals and solvents were used without any other purification.

Synthesis of $[Cu(TERPY)(H_2O)_2]^{2+}$ $[Cu(TERPY)(ADP)]^-$-$[H_2ADP]^-\cdot 16\ H_2O$

The salt $[MCHA]_2[HADP]$ (25 mg, 3.7×10^{-2} mmol) was added to a clear solution of TERPY (8.7 mg, 3.7×10^{-2} mmol) and 96% EtOH (1.5 mL). Water (20 drops) was added to the suspension to obtain the complete dissolution of $[MCHA]_2$-$[HADP]$. Copper sulfate pentahydrate (9 mg, 3.6×10^{-2} mmol) was dissolved in water (1 mL). The two solutions were mixed at room temperature. The final blue solution was heated for a few minutes at 70 °C. Single crystals suitable for X-ray diffraction were obtained by slowly evaporating the aqueous solution in an air atmosphere at room temperature. The crystals grew within 3 d from the mixing. They were collected, washed twice with cold water (5 mL each), twice with EtOH (3 mL each) and then stored in a sealed vessel at 5 °C. Yield 60%. Found: C, 34.02; H, 4.83; N, 12.8; P, 6.94. Calc. for $C_{25}H_{42}CuN_8O_{19}P_2$: C, 33.96; H, 4.79; N, 12.67; P, 7.01%.

Table 1 Crystal data and structure refinement for $[Cu(TERPY)(H_2O)_2]^{2+}[Cu(TERPY)(ADP)]^-[H_2ADP]^-\cdot 16H_2O$

Empirical formula	$C_{50}H_{84}Cu_2N_{16}O_{38}P_4$
M	1768.3
T/K	293(2)
λ/Å	0.71073
Crystal system, space group	Triclinic, $P\bar{1}$ (no. 1)
a/Å	12.171(2)
b/Å	13.098(2)
c/Å	14.221(3)
α/°	100.740(10)
β/°	104.32(2)
γ/°	115.380(10)
V/Å^3	1870.7(6)
Z	1
D_c/Mg m^{-3}	1.570
Reflections collected	6470 (R_{int} = 0.025)
Refinement method	Full-matrix least squares on F^2
Data/restraints/parameters	6440/0/1019
Goodness of fit on F^2	1.108
Final $R1$, $wR2$ [$I > 2\sigma(I)$]	0.0628, 0.1429
(all data)	0.0909, 0.2062
Absolute structure parameter	−0.01(2)
Largest difference peak and hole/e Å^{-3}	1.026 and −1.135

Infrared spectroscopy

The infrared spectra from KBr pellets were recorded on a Perkin-Elmer 1800 spectrometer.

X-Ray diffraction

X-Ray powder diffraction data were taken with Cu-Kα radiation (λ = 1.5418 Å, graphite monochromatized) on a Siemens D500 diffractometer. The generator was operated at 40 kV, 20 mA. Selected lines are (d, interplanar distance Å; relative intensity): 6.46, s (strong); 5.31, s; 3.38, s; 2.00, m (medium); 1.84, m; 1.76, m; 1.72, s.

Single crystal X-ray diffraction was performed on a blue plate (0.30 × 0.30 × 0.05 mm) chosen at the polarizing microscope and mounted on a glass fiber. Preliminary oscillation and Weissenberg photograms indicated that the crystal belonged to the triclinic system. The data collection was performed on a Siemens P4 diffractometer operating at 293 K. Crystallographic data are reported in Table 1. Unit cell parameters were obtained by least-squares refinement of the angles of 28 randomly selected reflections ($10 < 2\theta < 35°$). The intensities were corrected for Lorentz-polarization effects; absorption correction was performed through the ψ-scan technique. Reflections were considered observed [$I \geqslant 2\sigma(I)$]. The copper atoms and most of the atoms of the diphosphate chains of the nucleotide molecules were located through the direct methods of SHELXS 86.[15] A sequence of Fourier-difference analysis showed all the non-hydrogen atoms. The Fourier-difference map computed after an isotropic full-matrix least-squares refinement (10 cycles) of all the non-hydrogen atom positions allowed the location of H[C(2)], H_2[N(6A)], H[C(8)] for the adenine system of the metal-bound nucleotide molecule as well as H[N(1B)], H[C(2B)], H_2[N(6B)] and H[O(7)] for H_2ADP^-. The positions

Table 2 Bond lengths (Å) for $[Cu(TERPY)(H_2O)_2]^{2+}[Cu(TERPY)(ADP)]^{-}\cdot[H_2ADP]^{-}\cdot 16H_2O$

Cu(1)–O(3A)	2.244(10)	Cu(2)–O(1W2)	2.194(12)
Cu(1)–O(6A)	1.919(8)	Cu(2)–O(2W2)	1.939(8)
Cu(1)–N(11)	2.020(10)	Cu(2)–N(12)	2.021(11)
Cu(1)–N(21)	1.938(10)	Cu(2)–N(22)	1.950(9)
Cu(1)–N(31)	2.029(10)	Cu(2)–N(32)	2.042(11)
P(1A)–O(5′A)	1.594(9)	P(1B)–O(5′B)	1.592(7)
P(1A)–O(2A)	1.466(10)	P(1B)–O(2B)	1.484(9)
P(1A)–O(3A)	1.478(11)	P(1B)–O(3B)	1.494(9)
P(1A)–O(4A)	1.591(9)	P(1B)–O(4B)	1.616(10)
P(2A)–O(4A)	1.632(10)	P(2B)–O(4B)	1.602(8)
P(2A)–O(5A)	1.511(8)	P(2B)–O(5B)	1.483(9)
P(2A)–O(6A)	1.501(9)	P(2B)–O(6B)	1.483(9)
P(2A)–O(7A)	1.499(8)	P(2B)–O(7B)	1.539(11)
O(2′A)–C(2′A)	1.39(2)	O(2′B)–C(2′B)	1.401(14)
O(3′A)–C(3′A)	1.407(13)	O(3′B)–C(3′B)	1.411(12)
O(4′A)–C(1′A)	1.40(2)	O(4′B)–C(1′B)	1.404(15)
O(4′A)–C(4′A)	1.454(13)	O(4′B)–C(4′B)	1.448(13)
O(5′A)–C(5′A)	1.441(13)	O(5′B)–C(5′B)	1.454(13)
C(1′A)–C(2′A)	1.512(15)	C(1′B)–C(2′B)	1.526(15)
C(2′A)–C(3′A)	1.53(2)	C(2′B)–C(3′B)	1.532(13)
C(3′A)–C(4′A)	1.51(2)	C(3′B)–C(4′B)	1.52(2)
C(4′A)–C(5′A)	1.50(2)	C(4′B)–C(5′B)	1.52(2)
N(1A)–C(2A)	1.347(14)	N(1B)–C(2B)	1.351(15)
N(1A)–C(6A)	1.359(14)	N(1B)–C(6B)	1.363(14)
N(3A)–C(2A)	1.328(15)	N(3B)–C(2B)	1.324(15)
N(3A)–C(4A)	1.358(14)	N(3B)–C(4B)	1.373(13)
N(6A)–C(6A)	1.326(15)	N(6B)–C(6B)	1.314(14)
N(7A)–C(5A)	1.391(14)	N(7B)–C(5B)	1.403(14)
N(7A)–C(8A)	1.317(15)	N(7B)–C(8B)	1.314(14)
N(9A)–C(4A)	1.379(14)	N(9B)–C(4B)	1.378(13)
N(9A)–C(8A)	1.380(13)	N(9B)–C(8B)	1.375(13)
N(9A)–C(1′A)	1.460(13)	N(9B)–C(1′B)	1.471(13)
C(4A)–C(5A)	1.387(14)	C(4B)–C(5B)	1.361(14)
C(5A)–C(6A)	1.401(15)	C(5B)–C(6B)	1.39(2)

Table 3 Bond angles (°) for $[Cu(TERPY)(H_2O)_2]^{2+}[Cu(TERPY)(ADP)]^{-}[H_2ADP]^{-}\cdot 16H_2O$

O(3A)–Cu(1)–O(6A)	93.7(4)	O(1W2)–Cu(2)–O(2W2)	94.7(4)
O(3A)–Cu(1)–N(11)	94.9(4)	O(1W2)–Cu(2)–N(12)	96.9(5)
O(3A)–Cu(1)–N(21)	100.9(4)	O(1W2)–Cu(2)–N(22)	95.7(4)
O(3A)–Cu(1)–N(31)	92.7(4)	O(1W2)–Cu(2)–N(32)	93.0(5)
O(6A)–Cu(1)–N(11)	95.3(4)	O(2W2)–Cu(2)–N(12)	96.2(4)
O(6A)–Cu(1)–N(21)	164.9(4)	O(2W2)–Cu(2)–N(22)	169.3(5)
O(6A)–Cu(1)–N(31)	103.1(4)	O(2W2)–Cu(2)–N(32)	101.9(4)
N(11)–Cu(1)–N(21)	79.7(4)	N(12)–Cu(2)–N(22)	80.0(4)
N(11)–Cu(1)–N(31)	159.5(4)	N(12)–Cu(2)–N(32)	158.5(4)
N(21)–Cu(1)–N(31)	80.2(4)	N(22)–Cu(2)–N(32)	80.1(4)
P(1A)–O(3A)–Cu(1)	121.8(5)		
P(2A)–O(6A)–Cu(1)	134.5(5)		
C(211)–N(11)–Cu(1)	114.9(8)	C(212)–N(12)–Cu(2)	114.1(9)
C(611)–N(11)–Cu(1)	126.0(8)	C(612)–N(12)–Cu(2)	127.2(9)
C(221)–N(21)–Cu(1)	119.2(8)	C(222)–N(22)–Cu(2)	117.9(9)
C(621)–N(21)–Cu(1)	119.3(10)	C(622)–N(22)–Cu(2)	118.1(8)
C(231)–N(31)–Cu(1)	114.3(9)	C(232)–N(32)–Cu(2)	113.1(9)
C(631)–N(31)–Cu(1)	128.4(9)	C(632)–N(32)–Cu(2)	126.2(9)
O(2A)–P(1A)–O(3A)	118.1(6)	O(2B)–P(1B)–O(3B)	116.3(6)
O(2A)–P(1A)–O(4A)	111.4(5)	O(2B)–P(1B)–O(4B)	110.7(6)
O(2A)–P(1A)–O(5′A)	106.5(6)	O(2B)–P(1B)–O(5′B)	106.8(4)
O(3A)–P(1A)–O(4A)	109.9(5)	O(3B)–P(1B)–O(4B)	111.5(5)
O(3A)–P(1A)–O(5′A)	109.2(5)	O(3B)–P(1B)–O(5′B)	109.6(5)
O(4A)–P(1A)–O(5′A)	100.2(5)	O(4B)–P(1B)–O(5′B)	100.7(4)
O(5A)–P(2A)–O(4A)	103.3(5)	O(5B)–P(2B)–O(4B)	108.5(5)
O(6A)–P(2A)–O(4A)	106.1(5)	O(6B)–P(2B)–O(4B)	109.7(5)
O(6A)–P(2A)–O(5A)	113.2(6)	O(6B)–P(2B)–O(5B)	116.8(5)
O(7A)–P(2A)–O(4A)	106.2(5)	O(7B)–P(2B)–O(4B)	110.8(5)
O(7A)–P(2A)–O(5A)	114.9(5)	O(7B)–P(2B)–O(6B)	100.7(5)
O(7A)–P(2A)–O(6A)	112.1(5)	O(7B)–P(2B)–O(5B)	109.0(6)
P(1A)–O(4A)–P(2A)	131.0(5)	P(1B)–O(4B)–P(2B)	127.3(6)
C(5′A)–O(5′A)–P(1A)	119.9(9)	C(5′B)–O(5′B)–P(1B)	118.8(7)
C(2A)–N(1A)–C(6A)	118.5(9)	C(2B)–N(1B)–C(6B)	123.6(10)
C(2A)–N(3A)–C(4A)	110.7(9)	C(2B)–N(3B)–C(4B)	112.0(9)
C(5A)–N(7A)–C(8A)	104.6(9)	C(5B)–N(7B)–C(8B)	103.7(8)
C(4A)–N(9A)–C(8A)	105.3(9)	C(4B)–N(9B)–C(8B)	105.3(8)
C(4A)–N(9A)–C(1′A)	125.8(8)	C(4B)–N(9B)–C(1′B)	126.1(8)
C(8A)–N(9A)–C(1′A)	128.8(9)	C(8B)–N(9B)–C(1′B)	127.6(8)
N(3A)–C(2A)–N(1A)	129.3(10)	N(3B)–C(2B)–N(1B)	124.8(11)
N(3A)–C(4A)–C(5A)	126.2(10)	N(3B)–C(4B)–C(5B)	126.1(10)
N(9A)–C(4A)–C(5A)	106.6(9)	N(9B)–C(4B)–C(5B)	106.9(9)
N(9A)–C(4A)–N(3A)	127.0(9)	N(9B)–C(4B)–N(3B)	126.9(9)
C(4A)–C(5A)–C(6A)	117.6(10)	C(4B)–C(5B)–C(6B)	119.7(10)
C(4A)–C(5A)–N(7A)	109.8(9)	C(4B)–C(5B)–N(7B)	110.4(9)
N(7A)–C(5A)–C(6A)	132.4(9)	N(7B)–C(5B)–C(6B)	129.9(10)
N(6A)–C(6A)–N(1A)	119.4(10)	N(6B)–C(6B)–N(1B)	120.1(10)
N(6A)–C(6A)–C(5A)	122.9(11)	N(6B)–C(6B)–C(5B)	125.9(10)
N(1A)–C(6A)–C(5A)	117.5(9)	N(1B)–C(6B)–C(5B)	113.6(9)
N(7A)–C(8A)–N(9A)	113.4(10)	N(7B)–C(8B)–N(9B)	113.6(9)
C(1′A)–O(4′A)–C(4′A)	108.7(9)	C(1′B)–O(4′B)–C(4′B)	107.8(9)
O(4′A)–C(1′A)–N(9A)	108.5(10)	O(4′B)–C(1′B)–N(9B)	108.0(9)
O(4′A)–C(1′A)–C(2′A)	107.1(9)	O(4′B)–C(1′B)–C(2′B)	106.4(8)
N(9A)–C(1′A)–C(2′A)	114.9(9)	N(9B)–C(1′B)–C(2′B)	113.7(8)
O(2′A)–C(2′A)–C(1′A)	114.2(10)	O(2′B)–C(2′B)–C(1′B)	109.9(8)
O(2′A)–C(2′A)–C(3′A)	116.9(10)	O(2′B)–C(2′B)–C(3′B)	114.7(9)
C(1′A)–C(2′A)–C(3′A)	100.9(9)	C(1′B)–C(2′B)–C(3′B)	100.0(8)
O(3′A)–C(3′A)–C(4′A)	112.2(9)	O(3′B)–C(3′B)–C(4′B)	111.8(8)
O(3′A)–C(3′A)–C(2′A)	106.5(11)	O(3′B)–C(3′B)–C(2′B)	107.4(8)
C(4′A)–C(3′A)–C(2′A)	103.0(9)	C(4′B)–C(3′B)–C(2′B)	103.2(9)
O(4′A)–C(4′A)–C(3′A)	107.0(10)	O(4′B)–C(4′B)–C(3′B)	107.5(9)
O(4′A)–C(4′A)–C(5′A)	108.6(9)	O(4′B)–C(4′B)–C(5′B)	108.1(9)
C(3′A)–C(4′A)–C(5′A)	114.1(10)	C(3′B)–C(4′B)–C(5′B)	116.1(9)
O(5′A)–C(5′A)–C(4′A)	109.6(11)	O(5′B)–C(5′B)–C(4′B)	106.6(9)

of these H atoms were freely refined in the subsequent least-squares cycles. All the other H atoms of the adenosine diphosphate molecules and TERPY molecules were located and refined through the HFIX and AFIX options of SHELXL 93.[16] The H atoms of the H_2O ligand and H_2O free molecules were not located. The last stage of refinement consisted of full-matrix least-squares cycles (10) at the anisotropic level for the Cu, P, O, N, and C atoms. The H atoms were refined as isotropic with their thermal parameter restrained to 1.2 U_{eq} of the atom to which they are bound.

The choice of the absolute configuration was based on the value of the Flack parameter.[17] All the calculations were carried out on Pentium personal computers *via* SHELXS 86, SHELXL 93 and PARST 95[18] programs. Molecular graphics was performed with ZORTEP[19] and ORTEP 3 for Windows.[20]

Selected bond distances and angles are given in Tables 2 and 3.

CCDC reference number 186/1309.

See http://www.rsc.org/suppdata/dt/1999/699/ for crystallographic files in .cif format.

Computational procedure

All calculations have been performed by using the GAUSSIAN 94/DFT package.[21] Geometries, energetics and the population analysis reported were obtained using the B3LYP method.[22] We have mainly used the LANL2DZ basis set[21] which consists of the 6-31G like functions for non-transition metal ions and a valence double-zeta basis set for 3s, 3p, 3d and 4s electrons and orbitals along with an effective core potential (Hay and Wadt)[23] for the metals. In one case, namely $P_2O_7^{4-}$, the cc-pVDZ[24] basis set (correlation consistent polarized valence) was used. The aim of the present density functional computation was the simulation of the general conformation of diphosphate groups and metal–diphosphate complexes. The goal could be reached also by the simpler LANL2DZ basis set (see below, Results and Discussion). It should be noted that the inclusion of polarization functions for P and O (cc-pVDZ) improved the agreement between computed and experimental P–O bond distances but the P–O–P bond angle (160.5°) is far from the computed value

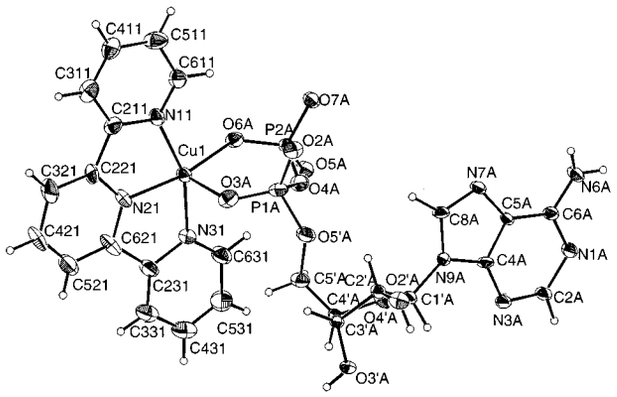

Fig. 1 Drawing of the $[Cu(TERPY)(ADP)]^-$ complex molecule with the labeling scheme. The ellipsoids enclose 30% probability.

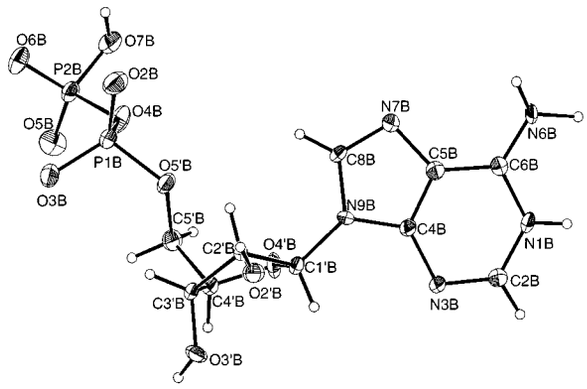

Fig. 2 Drawing of the H_2ADP^- molecule with the labeling scheme. The ellipsoids enclose 30% probability.

(180°)[25a] at the 6-31G**[25b] level. As the overall conformation of free and metal-bound diphosphates is reproduced at the more economic LANL2DZ level, we used this latter basis set for all the systems reported in this work.

All the geometrical parameters have been fully optimized. The system $[Zn(HP_2O_7)(NH_3)_2]^-\cdot NH_3$ was optimized to the convergence criteria of the Gaussian 94/DFT package for maximum force, rms force, and rms displacement. The maximum displacement was 0.0062 Å (limiting value for GAUSSIAN 94/DFT package, 0.0018); the total energy did not change more than 0.07 kcal in the last ten cycles (out of a total of 80). The structure was considered optimized at this stage. The $[Cu(HP_2O_7)(NH_3)_3]^-$ molecule was optimized to the convergence criteria for maximum force and rms force. The maximum displacement was 0.0089 Å and the rms displacement 0.0022 (limiting value for GAUSSIAN 94/DFT package, 0.0012); the total energy did not change more than 0.10 kcal in the last ten cycles (out of a total of 80). The geometry was considered optimized at this stage. All the other molecules or aggregates were fully optimized on the basis of the criteria implemented in the GAUSSIAN 94/DFT package.

Results and discussion

X-Ray crystallography

The asymmetric unit consists of $[Cu(TERPY)(H_2O)_2]$ $[Cu(TERPY)(ADP)][H_2ADP]\cdot 16H_2O$. The two copper atoms have different co-ordination spheres: Cu(1) is surrounded by two phosphate groups from an ADP^{3-} molecule and by three nitrogen atoms from a TERPY molecule; Cu(2) is co-ordinated to two water molecules and to three nitrogen atoms from a TERPY molecule. Both Cu(1) and Cu(2) have a pseudo-square pyramidal co-ordination environment. The H_2ADP^- anion has no covalent linkage to the metal centres. The ORTEP drawings are in Figs 1–3.

Diphosphate geometry and conformation. The bridging P–O bond lengths are 1.591(9) [P(α)–O] and 1.632(10) Å [O–P(β)] for copper-bound ADP^{3-} whereas they measure 1.616(10) and 1.602(8) for the non-coordinated H_2ADP^- molecule. An ADP–metal species studied *via* X-ray diffraction at a good accuracy contains K^+ cations.[26] For this latter case the H_2ADP^- molecule has mostly electrostatic interactions to the cations, and the P–O bridging distances [1.626(8), P(α)–O; 1.609(8) Å, O–P(β)] are very similar to that of H_2ADP^- of the present structure. Another good accuracy structure of H_2ADP^- contains $(HOCH_2)_3(CH_3)N^+$, Tris, cations.[27] In this case P(β)–O [1.627(5) Å] is longer than P(α)–O [1.585(6) Å].

The P–O–P bond angle is 131.0(5)° and 127.3(6)° for $[Cu(ADP)(TERPY)]^-$ and H_2ADP^-, respectively. The P(α)···P(β) distance is 2.933(7) and 2.884(7) for the same molecules. Relevant values found for ATP complexes are equal or larger than 2.90 Å (see refs. 12 and 28 and refs. therein). In the structure $KH_2ADP\cdot 2H_2O$[26] the P(α)···P(β) distance is 2.947(8) Å and $[(HOCH_2)_2(CH_3)N][H_2ADP]\cdot 2H_2O$[27] it is 2.916(8) Å. Angles of 131.3(4) and 130.5(3)° were reported for $KH_2ADP\cdot 2H_2O$ and $[(HOCH_2)_3(CH_3)N][H_2ADP]\cdot 2H_2O$. The angles around P(α) which involve the terminal oxygen atoms [namely O(2) and O(3)] are larger than the idealized tetrahedral value of 109.5, *i.e.* 118.1(6)° for $[Cu(ADP)(TERPY)]^-$ and 116.3(6) for H_2ADP^-. All the other values are close to 109.5°, except for O(5′)–P(α)–O(4) which is 100.2(5) and 100.7(4)° for $[Cu(ADP)(TERPY)]^-$ and H_2ADP^- respectively. The angles around P(β) have also significant deviations from the idealized values. The largest deviations are that of O(4)–P(2)–O(6) 103.3(5)° for $[Cu(ADP)(TERPY)]^-$ and that of O(4)–P(2)–O(7) 100.7(5)° for H_2ADP^-. It should be noted that the O(5A)–P(2A)–O(6A) angle for $[Cu(ADP)(TERPY)]^-$ is 113.2(6)°, O(6A) being strongly bound to copper (see below).

The P(α)–O–P(β)–O(6) torsion angle values are -38(1) and 24(1) for the copper-bound and free H_2ADP^- molecules, respectively. Therefore the conformation around the diphosphate chain is in the *gauche* and *cis* domain respectively on the basis of spectroscopic and crystallographic notations.[29]

The nucleoside molecule co-ordinated to the metal is reported as fully deprotonated, ADP^{3-}, whereas the free nucleoside molecule is protonated, H_2ADP^-, on the phosphate(β) and on the N(1) purine atom on the basis of several observations. The different protonation of the terminal phosphate group is related to the P–O bond distances. For the metal bound molecule the terminal P–O distances have almost the same value, 1.511(8) [P(2A)–O(5A)], 1.501(9) [P(2A)–O(6A)] and 1.499(8) Å [P(2A)–O(7A)]. The linkage of O(6A) to the metal does not influence much the value of P(2A)–O(6A). For the free nucleotide molecule the P(2B)–O bond distances are: P(2B)–O(5B) 1.483(9); P(2B)–O(6B) 1.483(9); P(2B)–O(7B) 1.539(11) Å. These values are consistent with monoprotonation

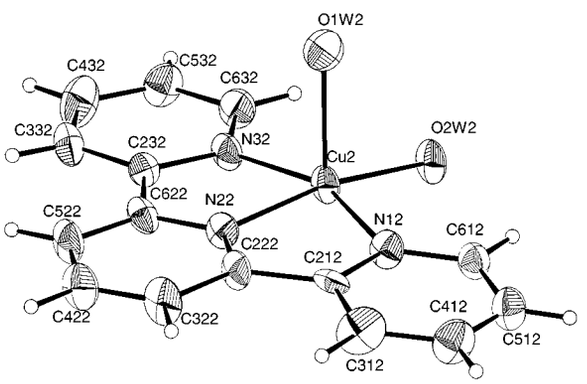

Fig. 3 Drawing of the $[Cu(TERPY)(H_2O)]^{2+}$ complex molecule with the labeling scheme. The ellipsoids enclose 30% probability.

of the terminal phosphate [namely O(7B)] of the free nucleotide molecule but not of the metal-bound nucleotide. The difference between the P(2B)–O(7B) distance and the lengths of the other two P(2B)–O(terminal) vectors is only 5.6 times the estimated standard deviation; however, the Fourier-difference map showed the hydrogen atom on O(7B) but not any hydrogen atom on the O(5A) or O(7A) atoms (see above, Experimental Section). Further observations on the protonation status of the nucleotide molecules are discussed below (see Hydrogen bonds, Interaggregate interactions and conclusion).

Metal co-ordination to diphosphate. The Cu(1) atom is co-ordinated to the diphosphate chain of a fully deprotonated ADP^{3-} molecule through one oxygen donor from both phosphate(α) [Cu(1)–O(3A) 2.24(1) Å] and phosphate(β) [Cu(1)–O(6A) 1.919(8) Å]. The metal centre is also linked to three nitrogen atoms from one TERPY ligand. The geometry of the co-ordination sphere can be described as square pyramidal. The equatorial donors are the three nitrogens from TERPY and O(6A); the apical donor is O(3A). The four equatorial donors are almost coplanar, deviations ranging from −0.07(1) [N(21)] to 0.07(1) Å [N(31)], whereas the metal centre deviates 0.1846(4) Å from the plane, towards O(3A). The angles formed by the apical Cu(1)–O(3A) vector with the equatorial Cu–N/O vectors are 93.7(4) [O(6A)], 94.9(4) [N(11)], 100.9(4) [N(21)] and 92.7° [N(31)]. The conformation of the six-membered co-ordination ring at the pyrophosphate chain can be described as boat with the O(4A) and Cu(1) atoms out of the plane defined by O(3)/P(1)/P(2)/O(6) by 0.467(9) and 0.2942(3) Å, respectively. A Cremer and Pople[30] conformation analysis of the same ring gives a total puckering amplitude Q_T 0.513(8) Å (0.630 Å for cyclohexane), a boat component θ 98.2(4)° (90 for pure boat, 0/180° for pure chair) and a skewing component φ −27.4(8)° (0 for pure boat, −90/90° for pure skewed boat). It is interesting that the α/β and β/γ chelate rings for $[M(HATP)_2]^{4-}$ anions have chair and skew boat conformation respectively.[12,31] The chelate ring of KH_2ADP[26] has a distorted chair conformation. The handedness of the co-ordination can be designed as Δ (see ref. 31 and refs. therein) for the present structure.

Geometry and conformation of the nucleoside moiety. The adenine system of the $[Cu(ADP)(TERPY)]^-$ anion is deprotonated at N(1), whereas the H_2ADP^- anion is protonated at the same position. This finding came from the analysis of the Fourier-difference map which showed a peak attributable to a proton for N(1) only in the case of the free nucleotide molecule. It is confirmed by the value of the C(2)–N(1)–C(6) angle which is 118.5(9) and 123.6(10)°, for the co-ordinated and free nucleotide molecules, respectively. It should be noted that Singh[32] reported an analysis of geometrical parameters for N(1)-protonated and non-protonated purine systems and concluded that C(2)–N(1)–C(6) angles are in the range 125 ± 3 and 116 ± 3° for the two cases, respectively. The N(1)–C(2)–N(3) angle is 129(1) and 125(1)° for metal-bound ADP^{3-} and free H_2ADP^- . Endocyclic N(6) angles differ by 3.9(9)°, the largest value being that for metal-bound nucleotide. The other corresponding angles differ by 3(1)° or less. Corresponding bond distances for the two adenine systems are almost equal, the largest difference being that relevant to C(4)–C(5) [1.39(1) and 1.36(1) Å for metal-bound ADP^{3-} and free H_2ADP^-, respectively]. The nine endocyclic atoms of the purine systems define good least-squares planes, the largest deviations being that of C(6B) [0.05(1) Å]. Atom N(6A) deviates slightly [0.087(2) Å] from the purine. Small deviations are also found for C(1′A) [0.06(2)] and C(1′B) [0.14(1) Å].

The conformations around the glycosidic bond N(9)–C(1′) for the nucleoside moieties of this structure are unusual. They are measured by the C(4)–N(9)–C(1′)–O(4′) (χ) torsion angle; χ is −84(1)° for the copper bound nucleotide molecule and −94(1)° for the free H_2ADP^- anion. So the conformation can be described as *high-anti*, *-sc*[33] and *anti*, *-ac* for metal-bound ADP^{3-} and H_2ADP^-, respectively. The extreme position described as *high-anti* is not frequent for nucleoside and it has never been found before for solid state structures of ATP and ADP nucleotides. The conformation of the ribose ring can be described on the basis of the pseudo-rotation phase angle *P* calculated from the endocyclic sugar torsion angles;[34] *P* is 161(1) and 151(1)° for metal-bound ADP^{3-} and H_2ADP^-, respectively so that the conformation of the sugar is pure *C(2′)-endo* (^{2}E, envelope) and *C(2′)-endo* with a small component of *C(1′)-exo* for the metal-bound and free nucleotide molecules, respectively. In fact the C(1′), C(3′), C(4′) and O(4′) atoms define a good least-squares plane for both the nucleotides [maximum deviation 0.005(11) Å for C(4′A)]. It should be noted that the pure *C(2′)-endo* conformation has never been found for ATP metal complexes, whereas it is very common for ADP metal complexes or ADP salts.[31] It would be interesting to crystallize a larger number of nucleoside diphosphate complexes to see if this conformation is the favorite one for this class of nucleotide. It was previously reported that the χ value is larger for *C(2′)-endo* than for a *C(3′)-endo* sugar conformation.[35] That finding is confirmed by the present work. The degree of pucker of the ribose ring based on the q_2 parameter[30] is similar for the two nucleotide molecules in the present structures [0.35(1) and 0.38(1) Å for metal-bound and free nucleotide, respectively].

The conformation around the C(4′)–C(5′) vector (Table 4) is *gauche-*, *gauche+* (*+sc*) for both the nucleotide molecules of the present structure on the basis of the ψ_{OO} [−68(1) and −75(1)° for A and B, respectively] and ψ_{OC} [51(1) (A) and 46(1)° (B)] torsion angles. The rotations around C(5′)–O(5′) (φ) and O(5′)–P(α) (ω) are *trans* and *gauche-* for both metal-bound ADP^3 and H_2ADP^-, respectively.

Table 4 Selected torsion angles (°) defining the ribose and the phosphate chain conformations

	Molecule A, $[Cu(TERPY)(ADP)]^-$	Molecule B, H_2ADP^-
φ C(4′)–C(5′)–O(5′)–P(1)	170.3(9)	−154.1(9)
ω C(5′)–O(5′)–P(1)–O(4)	−61(1)	62(1)
ψ_{OC} C(3′)–C(4′)–C(5′)–O(5′)	51(1)	46(1)
ψ_{OO} O(4′)–C(4′)–C(5′)–O(5′)	−68(1)	−75(1)
ψ C(5′)–C(4′)–C(3′)–O(3′)	147(1)	142(1)
χ C(4)–N(9)–C(1′)–O(4′)	−84(1)	−94(1)
τ_0 C(4′)–O(4′)–C(1′)–C(2′)	−23(1)	−29(1)
τ_1 O(4′)–C(1′)–C(2′)–C(3′)	35(1)	39(1)
τ_2 C(1′)–C(2′)–C(3′)–C(4′)	−33(1)	−33(1)
τ_3 C(2′)–C(3′)–C(4′)–O(4′)	21(1)	18(1)
τ_4 C(3′)–C(4′)–O(4′)–C(1′)	1(1)	7(1)
C(5′)–O(5′)–P(1)–O(2)	−177.6(1)	−177.9(9)
C(5′)–O(5′)–P(1)–O(3)	54(1)	55(1)
O(5′)–P(1)–O(4)–P(2)	174.7(8)	160.6(8)
O(2)–P(1)–O(4)–P(2)	-73(1)	−87(1)
O(3)–P(1)–O(4)–P(2)	60(1)	44(1)
P(1)–O(4)–P(2)–O(5)	−157.3(9)	−104.5(9)
P(1)–O(4)–P(2)–O(6)	−38(1)	24(1)
P(1)–O(4)–P(2)–O(7)	81(1)	141.0(9)

Structure of $[Cu(TERPY)(H_2O)_2]^{2+}$. The TERPY ligand acts as tridentate at three equatorial sites. One of the H_2O ligands occupies the fourth equatorial position and the other molecule is at the apical position.

The Cu–N bond distance relevant to the central pyridine ring of TERPY is 1.950(9) Å, shorter than the Cu–N bond lengths for the peripheral pyridine rings [average, 2.025(10) Å] in agreement with the values for $[Cu(ADP)(TERPY)]^-$ [Cu(1)–N(21) 1.938(10); Cu(1)–N(11) 2.020(10); Cu(1)–N(31) 2.029(10) Å]. The equatorial Cu–O(2W2) vector, 1.939(8) Å, is much shorter than the apical one, Cu–O(1W2) 2.194(12) Å. The

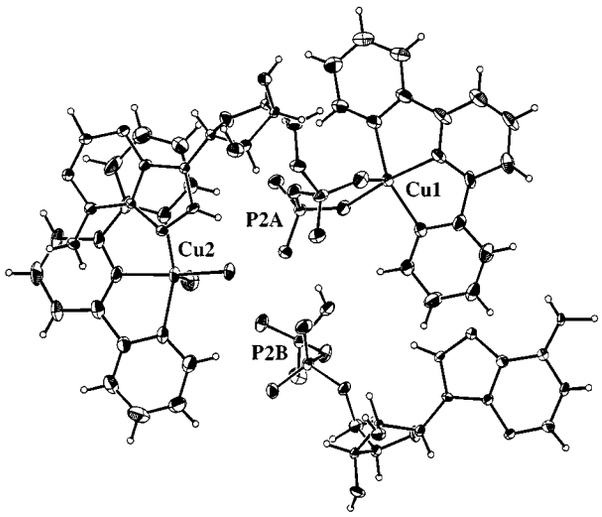

Fig. 4 Drawing of the $[Cu(TERPY)(H_2O)]^{2+}$ $[Cu(TERPY)(ADP)]^{-}$ H_2ADP^{-} self-assembly.

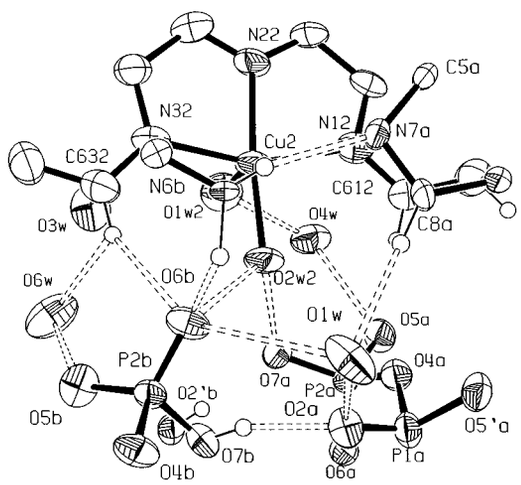

Fig. 5 All the atoms within a sphere (radius 6 Å) centred on O(2W2). Hydrogen bonds are represented by dashed lines.

four equatorial donors define a good plane, the largest deviation from the mean least-squares plane being that of N(22), 0.001(14) Å. The metal atom deviates 0.174(3) Å towards the apical position. The O(1W2)–Cu(2)–N angles are in the range 93.0(5)–96.9(5)°; whereas O(1W2)–Cu(2)–O(2W2) is 94.7°. The equatorial bond angles N–Cu–N(*cis*) are 80.0(4)° (average), whereas O(2W2)–Cu(2)–N(*cis*) are 96.2(4) and 101.9(4)°.

Bond distances and angles relevant to the Cu(TERPY) moieties in this work are in agreement with the values previously reported for copper(II)–TERPY complexes with analogous co-ordination environments.[36,37]

Supramolecular aggregates. Molecules of $[Cu(ADP)(TERPY)]^{-}$, $[Cu(TERPY)(H_2O)_2]^{2+}$, H_2ADP^{-} build supramolecular aggregates in 1 : 1 : 1 ratio (Fig. 4). Each superstructure is stabilized by a complicated web of electrostatic and hydrogen bonding interactions which mostly act at the central region of the unit. Stacking interactions between the aromatic rings co-operate to strengthen each aggregate. Free water molecules are mostly distributed around the hydrophilic regions of the nucleotides (pyrophosphate and sugar moieties) and around the $Cu–OH_2$ group. The triplets are connected to each other *via* stacking and hydrogen bonding interactions.

Hydrogen bonds and electrostatic interactions. Hydrogen bonds are listed in Table 5. The pyrophosphate groups of H_2ADP^{-} and $[Cu(ADP)(TERPY)]^{-}$ face each other and both face the $Cu(H_2O)_2$ region of $[Cu(TERPY)(H_2O)_2]^{2+}$ (Fig. 5). Selected hydrogen bonds which link the three molecules are: O(2A)···H–O(7B) [$d_{O\cdots O}$ 2.65(1)]; O(7A)···H–O(2W2) [2.60(1)]; O(6B)···H–O(2W2) [2.63(1)] and O(6B)···H–C(632) [$d_{O\cdots C}$, 3.35(1) Å]. The short O(2A)···O(7B) contact distance is in agreement with the presence of a hydrogen bond and hence with the protonation of O(7B), as O(2A) can be protonated only at a very low pH. The short O(7A)···O(2W2) contact distance can be explained with the presence of a hydrogen bond in which O(2W2) is the hydrogen donor but it does not exclude that O(7A) is protonated and O(2W2) is the hydro-

Table 5 Selected contact distances (Å) indicative of possible hydrogen bonds

		Equivalent position
O(2A)···O(7B)	2.65(1)	x, y, z
O(7A)···H–O(2W2)	2.60(1)	
O(6B)···H–O(2W2)	2.63(1)	
O(6B)···C(632)	3.35(1)	
O(4W)···O(5A)	2.71(2)	
O(4W)···O(1W2)	2.72(2)	
O(8W)···C(312)	3.27(3)	
O(7W)···C(512)	3.24(2)	
O(3W)···O(9W)	2.74(2)	
O(5W)···O(13W)	2.92(3)	
O(8W)···O(10W)	2.93(3)	
O(8W)···O(15W)	2.68(2)	
O(9W)···O(15W)	2.75(4)	
O(10W)···N(1A)	2.80(3)	
O(10W)···O(12W)	2.67(2)	
O(11W)···O(14W)	2.88(3)	
O(1W)···C(8A)	3.26(2)	$x - 1, y, z$
N(7B)···N(6A)	2.97(1)	$x, y + 1, z$
O(3B)···N(1B)	2.66(2)	
O(6B)···N(6B)	2.79(1)	
N(7A)···N(6B)	2.93(1)	$x, y - 1, z$
O(3A)···O(8W)	2.74(2)	
O(2′A)···O(12W)	3.00(2)	
O(13W)···O(16W)	2.72(3)	
O(2′A)···O(5W)	2.88(1)	$x + 1, y, z$
O(2′B)···O(7A)	2.70(1)	
O(2A)···O(1W)	2.77(2)	
O(6B)···O(1W)	3.33(2)	
O(3′A)···N(3B)	2.94(1)	$x - 1, y, z - 1$
O(6W)···C(632)	3.28(2)	
O(7W)···O(14W)	2.85(2)	
O(13W)···O(14W)	2.81(2)	
O(3′B)···N(3A)	2.78(1)	$x + 1, y, z + 1$
O(3B)···O(9W)	2.79(1)	
O(5B)···O(6W)	2.77(2)	
O(5B)···O(5W)	2.74(2)	
O(11W)···O(15W)	2.76(3)	
N(6A)···O(2W)	2.92(1)	$x + 1, y + 1, z$
O(3W)···O(1W2)	2.72(1)	$x, y, z - 1$
O(3′A)···O(5W)	2.92(1)	$x + 1, y, z$
O(2B)···O(1W)	2.77(2)	
O(2B)···O(2W)	2.82(2)	
O(2B)···O(4W)	2.81(2)	
O(3W)···O(6W)	2.76(3)	
O(3W)···O(16W)	2.92(3)	
O(10W)···O(16W)	3.09(4)	
O(3′B)···O(6W)	2.76(2)	$x + 2, y, z + 1$
O(1W)···O(12W)	2.75(3)	$x - 1, y - 1, z$
O(7W)···O(12W)	2.69(3)	

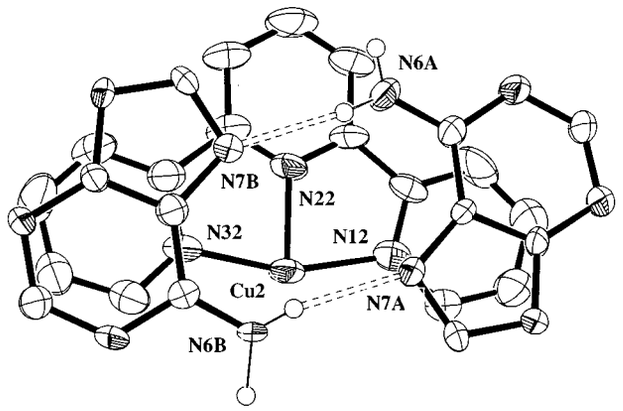

Fig. 6 Aromatic systems involved in the stacking interactions and in the adenine–adenine base pairing. Adenine B is at $x, y - 1, z$.

Table 6 Significant stacking distances (Å) between adenine A (copper-bound ADP^{3-}), adenine B (free H_2ADP^-) and the TERPY ligand of $[Cu(TERPY)(H_2O)_2]^{2+}$

Adenine A		Adenine B ($x, y - 1, z$)	
N(1A)···C(312)	3.48(3)	N(1B)···C(532)	3.55(3)
		N(1B)···C(632)	3.51(3)
C(2A)···C(312)	3.57(3)	C(2B)···C(532)	3.40(3)
C(2A)···C(412)	3.63(3)		
N(3A)···C(412)	3.51(3)	N(3B)···C(432)	3.52(3)
N(3A)···C(512)	3.70(2)	N(3B)···C(532)	3.52(2)
C(4A)···C(512)	3.51(2)	C(4B)···C(332)	3.64(2)
C(4A)···C(612)	3.64(2)	C(4B)···C(432)	3.48(3)
		C(4B)···C(532)	3.64(2)
C(5A)···N(12)	3.52(1)	C(5B)···N(32)	3.55(2)
C(5A)···C(212)	3.64(2)	C(5B)···C(232)	3.65(2)
		C(5B)···C(632)	3.65(2)
C(6A)···C(212)	3.46(2)	C(6B)···N(32)	3.64(2)
C(6A)···C(312)	3.65(3)	C(6B)···C(632)	3.45(2)
N(6A)···N(22)	3.53(2)		
N(6A)···C(222)	3.38(2)		
N(6A)···C(322)	3.57(3)		
N(7A)···N(12)	3.56(2)	N(7B)···C(232)	3.55(2)
C(8A)···C(612)	3.67(3)		
N(9A)···C(612)	3.67(2)	N(9B)···C(332)	3.62(2)

gen acceptor. Some free water molecules, particularly O(1W), O(3W), O(4W) and O(6W), also play an important role in stabilizing the triplet. Selected bonding distances are: O(1W)···O(2A) [$d_{(O\cdots O)}$ 2.77(2)]; O(1W)···O(6B) [3.33(2)]; O(1W)···H–C(8A) [$d_{(O\cdots C)}$ 3.26(2)]; O(4W)···O(5A) [$d_{(O\cdots O)}$ 2.71(2)]; O(4W)···O(1W2) [2.72(2)]; O(6W)···O(5B) [2.77(2)] and O(6W)···H–C(632) [$d_{(O\cdots C)}$ 3.28(2)].

Stacking interactions. The adenine system of [Cu(TERPY)-(ADP)]$^-$ and the TERPY ligand of $[Cu(TERPY)(H_2O)_2]^{2+}$ are connected by stacking interactions (Fig. 6 and Table 6) which reinforce the supramolecular aggregate. Selected short contact distances are: N(7A)···N(12) [3.56(2)]; C(5A)···C(212) [3.64(2)] and N(6A)···C(222) [3.38(2) Å] (note the strong effect at 3.38 Å in the X-ray diffraction powder diagram; see above, Experimental Section). The dihedral angle between the N(12)/C(212)/C(312)/C(412)/C(512)/C(612) and the least-squares planes of the adenine system of metal-bound ADP^{3-} is 1.4(5)°.

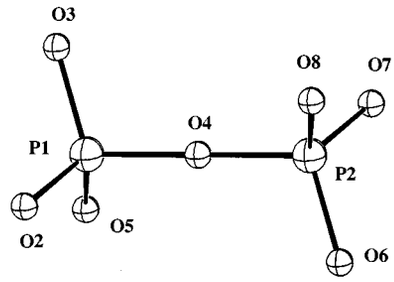

Fig. 7 Drawing of the fully optimized $P_2O_7^{4-}$ molecule at the B3LYP/LANL2DZ level.

Interaggregate interactions and base pairing. The aggregates interact with each other *via* hydrogen bonds and stacking interactions. The adenine system from metal-bound ADP^{3-}(A) and free H_2ADP^-(B) (this latter is from an outer aggregate) are paired *via* N(6A)H_2···N(7B) [$d_{(N\cdots N)}$ 2.97(1) Å] and N(6B)H_2···N(7A) [$d_{(N\cdots N)}$ 2.93(1) Å], see Fig. 6. It is interesting that the same adenine–adenine base-pairing scheme was previously found by one of us for the structure of $[Mg(H_2O)_6]$-[HDPA][$Mg(HATP)_2$]·$12H_2O$ (HDPA = protonated 2,2′-dipyridylamine)[12] and related compounds.[28,38] Atom N(1B) has a strong and interaggregate interaction with O(3B) [$d_{(N\cdots O)}$ 2.66(1) Å]. This short contact distance is consistent with the protonation of N(1B) of the free nucleotide molecule as the terminal oxygen atoms of the phosphate(*α*) can be protonated only at very low pH.

The two paired adenine systems are anchored to the same $[Cu(TERPY)(H_2O)_2]^{2+}$ molecules *via* stacking interactions. Some short stacking contacts which connect two aggregates are: N(1B)···C(632) 3.514(9); C(2B)···C(532) 3.404(9); C(5B)···C(232) 3.65(2) Å.

Infrared spectroscopy

The infrared spectrum has a band at 1649 cm^{-1} (strong, broad), which can be related to the scissoring mode of NH_2 proximal to deprotonated N(1).[12] The corresponding band for N(1) deprotonated Na_2HADP is located at 1663 cm^{-1}. The absence of an intense band at around 1700 attributable to the N(1)-protonated adenine NH_2 group can be related to the hydrogen bonds which involve NH_2 as well as N(1)H, see above, hydrogen bonding network.

The bands relevant to the PO_2 stretching modes occur at around 1230 and 1100 cm^{-1} as for adenosine 5′-triphosphate complexes.[12]

Molecular orbital calculations

Geometry. The selected geometrical parameters for all the molecules optimized in this work are shown in Table 7. The structures of $P_2O_7^{4-}$, $HP_2O_7^{3-}$, [Cu{*O*,*O*-PO_4}]$^-$, [Cu{*O*(*α*),*O*(*β*)-P_2O_7}]$^{2-}$, [Zn{*O*(*α*),*O*(*β*)-HP_2O_7}$(H_2O)(OH)]^{2-}$, [Zn{*O*(*α*),*O*(*β*)-HP_2O_7}$(NH_3)_2]^-$·NH_3 and [Cu{*O*(*α*),*O*(*β*)-HP_2O_7}$(NH_3)_3]^-$ are shown in Figs. 7–13.

$P_2O_7^{4-}$. The optimized structure for $P_2O_7^{4-}$ (Fig. 7) has a linear P–O–P bridge and the two PO_3 groups are staggered. The P–O(b) (b = bridge) and P–O(t) (t = terminal) distances are 1.793 and 1.659 Å, respectively. The computed bond distances are significantly longer than the corresponding ones found in the solid state for a variety of hydrogen orthophosphates, pyrophosphates, triphosphates and linear and cyclic metaphosphates [P-O(b) 1.61; P-O(t) 1.52].[39] It is interesting that some divalent cobalt ($Co_2P_2O_7$[40a]), nickel ($Ni_2P_2O_7$[40b]) and magnesium [$Nb_2Mg(P_2O_7)_3$[40c]] diphosphates have linear P–O–P bridges in the solid state. A certain overestimation of bond distances produced by the level of theory and basis set used for this work appears also from comparison with more sophisticated basis sets used recently for computations on magnesium

Table 7 Selected bond lengths (Å) and angles (°) (t, terminal; b, bridging; d, donor) of molecules calculated at the B3LYP/LANL2DZ level

System	O–H	N–H	P(1)–O(t)	P(1)–O(d)	P(1)–O(b)	P(2)–O(b)	P(2)–O(t)	P(2)–O(H)	P(2)–O(d)	M–O(P)	M–OH	M–NH_3	P–O–P	P–O–H	O(P)–M–O(P)
H_2O	0.977														
OH^-	1.005														
NH_3		1.088													
PO_4^{3-}			1.695												
$P_2O_7^{4-}$			1.659		1.793	1.793	1.659						179.7		
$HP_2O_7^{3-}$	1.096		1.631		1.824	1.756	1.627	1.723					133.0	109.7	
$[Cu(PO_4)]^-$			1.663	1.686						2.031					79.7
$[Cu(P_2O_7)]^{2-}$			1.607	1.760	1.766	1.766	1.607		1.760	1.837			158.6		148.8
$[Zn(P_2O_7)]^{2-}$			1.603	1.760	1.846	1.844	1.603		1.760	1.894			177.1		160.7
$[Cu(HP_2O_7)(NH_3)_3]^-$	0.982	1.033	1.606	1.694	1.828	1.698	1.624	1.720		1.934		2.070	138.7	110.2	
$[Zn(HP_2O_7)(H_2O)(OH)]^{2-}$	0.996 1.004 (H_2O) 1.027 ($HP_2O_7^{3-}$)		1.610	1.700	1.833	1.707	1.588	1.713	1.678	2.003	1.924 2.727 (H_2O)		138.3	112.7	100.0
$[Zn(HP_2O_7)(NH_3)_2]^-\cdot NH_3$	0.982	1.042 1.027 (free NH_3)	1.607	1.686	1.856	1.698	1.599	1.723	1.656	1.992		2.092	132.7	110.1	99.0

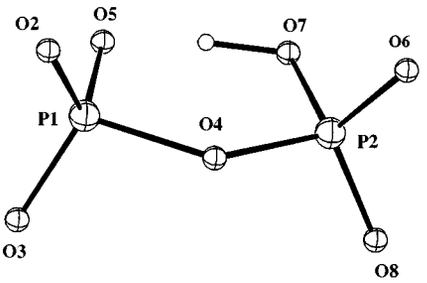

Fig. 8 Drawing of the fully optimized $HP_2O_7^{3-}$ molecule at the B3LYP/LANL2DZ level.

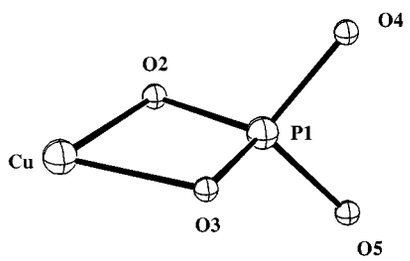

Fig. 9 Drawing of the fully optimized $[Cu(O,O\text{-}PO_4)]^-$ chelate at the B3LYP/LANL2DZ level.

and calcium pyrophosphates.[25a] Some enlarging effects (*ca.* 0.08 Å) for computed Zn–OH_2 bond distances in the gas phase when compared with experimental solid state ones for four-co-ordinate zinc(II) complexes were also noted in a previous work.[41]

$HP_2O_7^{3-}$. An optimized structure with a strong intramolecular hydrogen bond between the two PO_3 groups was computed in this work (Fig. 8). The conformation of the PO_3 groups is almost eclipsed [O(t)P···PO(t), *ca.* 3°]. The P–O(t) bond distances for the P(1) and P(2) atoms average 1.629 Å. The P(1)–O(b) and P(2)–O(b) distances are 1.824 and 1.756 Å, respectively. The last values are significantly different, and the trend is in agreement with the findings previously reported.[25a,42] The P–O–P angle is 133.0°.

A comparison of the computed structures of pyrophosphates from this work and those of previous molecular orbital calculations[25a,42] performed through the 6-31G** basis set as well as those from experimental solid state studies shows that our computational procedure reproduces well the general conformation of the ligand moiety, *i.e.* bond angles and torsion angles. The agreement for bond distances is not excellent (*e.g.* differences of some 0.10 Å for $P_2O_7^{4-}$) but it increases when the overall charge of the molecule decreases. For these reasons we may conclude that the B3LYP/LANL2DZ level is accurate enough (see above, computational procedure for the inclusion of polarization functions) for the purpose of computing bond angles and torsion angles of complex molecules such as $[M^{II}\{O(\alpha),O(\beta)\text{-}P_2O_7\}]^{2-}$ and $[M^{II}\{O(\alpha),O(\beta)\text{-}HP_2O_7\}(NH_3)_3]^-$ which can be considered models also for some metal–nucleoside 5′-diphosphate co-ordination compounds. Furthermore, relative effects on computed bond lengths such as protonation and metal co-ordination can be discussed even though absolute values are overestimated.

$[Cu(O,O\text{-}PO_4)]^-$. The optimization of the $[Cu\text{–}O\text{–}PO_3]^-$ molecule did not reach convergence. On the contrary the $[Cu(O,O\text{–}PO_4)]^-$ chelate molecule nicely converged to C_{2v} symmetry (Fig. 9). The Cu–O bond lengths are 2.031 Å, whereas the P–O(d) (d = donor) and P–O(t) bond lengths are 1.689 and 1.663 Å, respectively. The O–Cu–O bond angle is 79.7°.

$[Cu\{O(\alpha),O(\beta)\text{-}P_2O_7\}]^{2-}$. The starting structure had the two PO_3 groups eclipsed and the geometry optimization converged to the structure (whose symmetry is C_s) in Fig. 10. The Cu–O bond lengths are 1.837 Å, shorter than those for $[Cu(O,O\text{-}PO_4)]^-$, consistent with a smaller tension for the

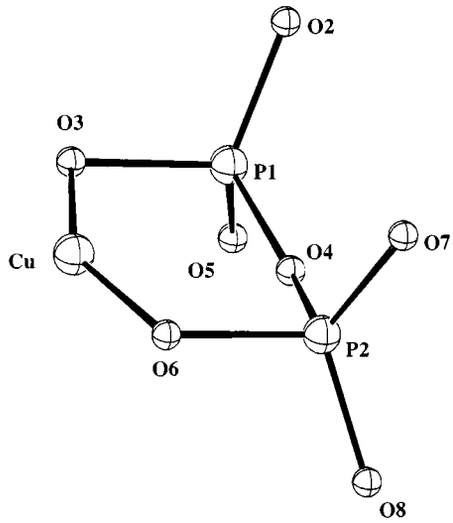

Fig. 10 Drawing of the fully optimized $[Cu\{O(\alpha),O(\beta)\text{-}P_2O_7\}]^{2-}$ chelate at the B3LYP/LANL2DZ level.

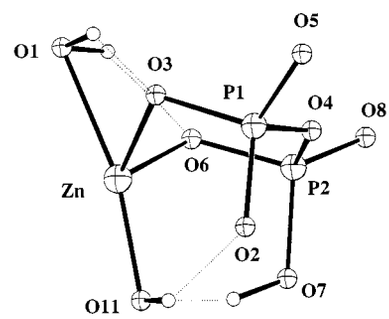

Fig. 11 Drawing of the fully optimized $[Zn\{O(\alpha),O(\beta)\text{-}HP_2O_7\}(H_2O)(OH^-)]^{2-}$ chelate at the B3LYP/LANL2DZ level.

six-membered chelate ring when compared to a four-membered one. The P–O(d) distances are 1.760 Å whereas the P–O(t) are 1.607 Å. The P–O(b) lengths are 1.766. The metal co-ordination to the two PO_3 groups slightly decreases the P–O(b) distances (some 0.03 Å) as well as the P–O(t) distances (some 0.06 Å). The P–O(d) distances increase by some 0.10 Å when compared to those of $P_2O_7^{4-}$. The P–O–P angle for computed $[Cu\{O(\alpha),O(\beta)\text{-}P_2O_7\}]^{2-}$ is 158.6°, much larger than the value found for $[Cu(TERPY)(ADP)]^-$ [131.0(5)°]. The discrepancy can be related to the difference in the co-ordination spheres. The conformation of the chelate ring for the computed structure is boat-envelope (Q_T 0.210 Å, φ 179.9°, θ 65.5° θ 90° for pure boat, 45° for pure envelope).

$[Zn\{O(\alpha),O(\beta)\text{-}P_2O_7\}]^{2-}$. The optimized structure of $[Zn\{O(\alpha),O(\beta)\text{-}P_2O_7\}]^{2-}$ has some significant differences when compared to $[Cu\{O(\alpha),O(\beta)\text{-}P_2O_7\}]^{2-}$. The P–O–P bridge [angle, 177.1°; O(b) displaced towards Zn] is almost linear as for $P_2O_7^{4-}$ and the chelate ring is very flat. The Zn–O distances (1.894 Å) are longer than the Cu–O ones (1.837 Å). The P–O(b) distance for the zinc species (1.845 Å) is much longer than the corresponding value for the copper species (1.766 Å). It is noteworthy that for $[Zn\{O(\alpha),O(\beta)\text{-}P_2O_7\}]^{2-}$ the Zn–O(b) distance is 2.042 Å and the O–Zn–O angle is 160.7°, in agreement with a Zn–O(b) bonding interaction.

$[Zn\{O(\alpha),O(\beta)\text{-}HP_2O_7\}(H_2O)(OH)]^{2-}$. An initial structure for $[Zn\{O(\alpha),O(\beta)\text{-}P_2O_7\}(H_2O)_2]^{2-}$ where the zinc ion has a pseudo-C_{2v} co-ordination environment was submitted to geometry optimization. During the refinement one of the co-ordinated water molecules lost a H atom which passed to P_2O_7. Thus, the final co-ordination sphere consists of a $O(\alpha),O(\beta)$-$HP_2O_7^{3-}$ chelating ligand, a OH^- anion and a H_2O molecule (Fig. 11). The Zn–OH and Zn–OH_2 bond distances are 1.924 and 2.272 Å, respectively; *i.e.* the water molecule is very weakly

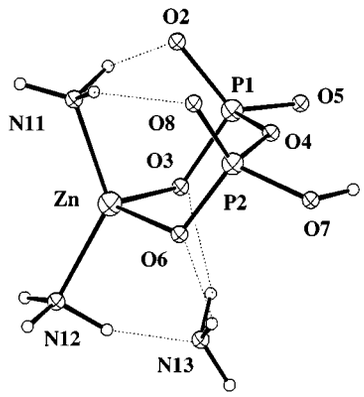

Fig. 12 Drawing of the partially optimized (see computational procedure) structure of the $[Zn\{O(\alpha),O(\beta)\text{-}HP_2O_7\}(NH_3)_2]^-\cdot NH_3$ aggregate at the B3LYP/LANL2DZ level.

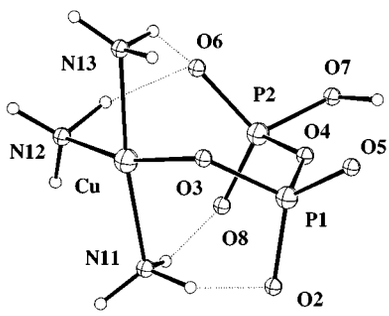

Fig. 13 Drawing of the partially optimized (see computational procedure) structure of the $[Cu\{O(\alpha),O(\beta)\text{-}HP_2O_7\}(NH_3)_3]^-$ complex molecule at the B3LYP/LANL2DZ level.

co-ordinated. The protons of the H_2O ligand interact with the oxygen donors from pyrophosphate. The P–O(d) distances average 1.700 Å whereas P(1)–O(b) and P(2)–O(b) are 1.833 and 1.707 Å, respectively. The conformation of the co-ordination ring is chair (Q_T 0.812 Å; φ 6.8°; θ 29.8°).

[Zn{O(α),O(β)-HP$_2$O$_7$}(NH$_3$)$_2$]$^-$·NH$_3$. A structure for $[Zn\{O(\alpha),O(\beta)\text{-}HP_2O_7\}(NH_3)_3]^-$ with pseudo-C_s symmetry was submitted to geometry optimization. The final partially optimized (see above, computational procedure) system (Fig. 12) has a four-co-ordinate zinc atom linked to two ammonia molecules and to two oxygen atoms from pyrophosphate. The co-ordination sphere is pseudo-tetrahedral. One of the ammonia molecules initially bound to zinc escaped the co-ordination sphere and linked to one co-ordinated ammonia molecule and to the two oxygen donors *via* hydrogen bonds. The P–O–P bond angles for both $[Zn\{O(\alpha),O(\beta)\text{-}HP_2O_7\}(H_2O)(OH)]^{2-}$ (138.3°) and $[Zn\{O(\alpha),O(\beta)\text{-}HP_2O_7\}(NH_3)_2]^-\cdot NH_3$ (132.7°) are in agreement with the solid state structure of [Cu(TERPY)(ADP)]$^-$ [131.0(5)°].

[Cu{O(α),O(β)-HP$_2$O$_7$}(NH$_3$)$_3$]$^-$. A structure for $[Cu\{O(\alpha),O(\beta)\text{-}HP_2O_7\}(NH_3)_3]^-$ with pseudo-C_s symmetry was submitted to geometry optimization. The partially optimized geometry (see above, computational procedure) is a four-co-ordinate, almost square planar, (Fig. 13), the metal atom being linked to three NH_3 molecules and to one oxygen atom of phosphate(1) [Cu–O(3), 1.934 Å]. The protonated phosphate escapes the co-ordination sphere and makes hydrogen bonds with the two *trans* NH_3 ligands. The P–O(b) bond distances are 1.828 [P(1)] and 1.698 Å [P(2)], and the P–O–P bond angle is 138.7°. The Cu–N bond distances are 2.03, 2.08, and 2.09 Å for N *cis*, *cis*, and *trans* to the O donor.

Metal-ligand binding energy. The calculated energies of some protonation and metal–ligand bond formation are in Table 8. It is evident that the formation energy for the $[Cu(O,O\text{-}PO_4)]^-$ chelate (−962.22 kcal mol^{-1}) is much smaller than the corresponding binding energy for $[Cu\{O(\alpha),O(\beta)\text{-}P_2O_7\}]^{2-}$ (-1071.66 kcal mol^{-1}). This is consistent with a higher strain energy for a four-membered chelate ring when compared to a six-membered one.

The formation of the 1:1 chelate system for zinc(II) is less favored than for copper(II). In fact the geometry optimization of $[Zn(O,O\text{-}PO_4)]^-$ did not converge, whereas the binding formation energy for $[Zn\{O(\alpha),O(\beta)\text{-}P_2O_7\}]^{2-}$ is −1017.88 kcal mol^{-1}, some 54 kcal smaller than the corresponding one for the copper(II) species.

Atomic charges. The atomic charges calculated through the Mulliken population analysis are shown in Table 9. The atomic charge of P in $P_2O_7^{4-}$ (1.442 e) is, as expected, higher than in PO_4^{3-} (1.330). The protonation of one of the PO_3 groups, as in $HP_2O_7^{3-}$, produces a decrease of the charge for both the phosphorus atoms (1.405, 1.418 e), even though P from protonated PO_3 is slightly more positive than the other.

The effect of metal chelation does not influence much the charge of P: 1.448 e for $[Cu\{O(\alpha),O(\beta)\text{-}P_2O_7\}]^{2-}$ and 1.399 for $[Cu(O,O\text{-}PO_4)]^-$. The chelation of Zn^{2+} by $P_2O_7^{4-}$ causes a small decrease of charge on P (down to 1.411 from 1.442). The atomic charge of copper is decreased to 0.361 e upon chelation by PO_4^{3-} and to 0.478 upon chelation by $P_2O_7^{4-}$. The electron donation to zinc by $P_2O_7^{4-}$ is much smaller than that to copper (charge of Zn, 1.00 e).

Vibrational frequencies. Selected normal frequencies, IR intensities and diagonal elements of the force constant matrix for $P_2O_7^{4-}$ and $[Cu\{O(\alpha),O(\beta)\text{-}P_2O_7\}]^{2-}$ calculated at the B3LYP/LANL2DZ level are listed in Table 10. A detailed discussion of the absolute values of vibrational frequencies for the stretching modes is not appropriate because bond distances are often overestimated at this level. However, a brief comparative analysis is reported mostly to understand the effect of complexation.

Upon complexation to copper the computed ν[P–O(t)] stretching frequency of $P_2O_7^{4-}$ is blue shifted by some 80 cm^{-1} in agreement with a significant shortening (0.052 Å) of the P–O(t) bond distance. The ν[P–O(b)] frequency is red shifted by some 40 cm^{-1} even though the computed P–O(b) bond distance undergoes a small shortening (0.028 Å). It should be noted that ν[P–O(b)] and ν[Cu–O] stretching modes are coupled in the case of $[Cu\{O(\alpha),O(\beta)\text{-}P_2O_7\}]^{2-}$.

Conclusion

This is the first structure of a nucleoside 5′-diphosphate (and -triphosphate) which contains covalently metal-bound and free nucleotide molecules. This allows a fine comparative analysis of the effects by metal co-ordination on the nucleotide. A copper(II) promoted dephosphorylation of ADP in aqueous solution has been previously presented.[43] It has been postulated that the dephosphorylation process proceeds *via* the formation of dimers which contain self-stacked adenine bases bound to metal centres through N(7). The present work confirms the formation of aggregates which contain two metal centres and two nucleotide molecules. The presence of a strong co-ordinating agent, TERPY in this work, makes only the co-ordination at the diphosphate possible; adenine nitrogen atoms are not involved. The TERPY–adenine stacking interaction and adenine–adenine base pairing play a very important structuring role to held diphosphates and copper(II) centres directly linked or bound *via* Cu–$OH_2\cdots$O(phosphate) bridges. Free water molecules are near the P(β) atom for the free nucleotide [P(2B)$\cdots$O(6W) 3.91(1) Å] and P(α) atom of the copper(II)-bound nucleotide [P(1A)$\cdots$O(1W) 3.80(1)]; the sum of the van der Waals radii for O and P is 3.35 Å.[44]

The copper(II)-bound O(2W2) water molecule is at 3.60(1) Å from P(β) of the copper(II)-bound nucleotide. Interestingly, the

Table 8 Bond formation energies (kcal mol^{-1}) for formal reactions calculated at the B3LYP/LANL2DZ level

Reaction	ΔE
$P_2O_7^{4-} + H^+ \longrightarrow HP_2O_7^{3-}$	−636.48
$Cu^{2+} + PO_4^{3-} \longrightarrow [Cu(O,O\text{-}PO_4)]^-$	−962.22
$Cu^{2+} + P_2O_7^{4-} \longrightarrow [Cu\{O(\alpha),O(\beta)\text{-}P_2O_7\}]^-$	−1071.66
$Zn^{2+} + P_2O_7^{4-} \longrightarrow [Zn\{O(\alpha),O(\beta)\text{-}P_2O_7\}]^-$	−1017.88
$Zn^{2+} + HP_2O_7^{3-} + OH^- + H_2O \longrightarrow [Zn\{O(\alpha),O(\beta)\text{-}HP_2O_7\}(H_2O)(OH)]^{2-}$	−876.88
$Zn^{2+} + HP_2O_7^{3-} + 3NH_3 \longrightarrow [Zn\{O(\alpha),O(\beta)\text{-}HP_2O_7\}(NH_3)_2]^-\cdot NH_3$	−879.88[a]
$Cu^{2+} + HP_2O_7^{3-} + 3NH_3 \longrightarrow [Cu\{O(\beta)\text{-}HP_2O_7\}(NH_3)_3]^-$	−927.08[a]

[a] The systems were geometry optimized without reaching the full convergence criteria of the GAUSSIAN 94/DFT package.

Table 9 Atomic charges (e) from the Mulliken population analysis calculated at the B3LYP/LANL2DZ level

System	O(H)	O(t)	O(b)	O(d)	N	P	P(OH)	Cu	Zn	H(O)	H(N)
										0.356	
H_2O	−0.711									0.144	
OH^-	−1.144										
Cu^{2+}								2			
Zn^{2+}									2		
NH_3					−0.893						0.298
PO_4^{3-}		−1.083				1.330					
$P_2O_7^{4-}$		−0.993	−0.926			1.442					
$HP_2O_7^{3-}$	−0.864	−0.902	−0.863			1.405	1.418			0.416	
$[Cu(PO_4)]^-$		−0.620		−0.760		1.399		0.361			
$[Cu(P_2O_7)]^{2-}$		−0.756	−0.892	−0.728		1.448		0.478			
$[Zn(P_2O_7)]^{2-}$		−0.781	−0.979	−0.862		1.411			1.003		
$[Cu(HP_2O_7)(NH_3)_3]^-$	−0.740	−0.777	−0.853	−0.789	−0.909	1.452	1.488	0.546		0.401	0.372
$[Zn(HP_2O_7)(H_2O)(OH)]^{2-}$	−0.770	−0.837	−0.825	−0.853		1.426	1.480		0.909	0.421	
	−0.895 (OH^-)			−0.895 (OH^-)						0.393 (OH^-)	
	−0.788 (H_2O)			−0.798 (H_2O)						0.424 (H_2O)	
$[Zn(HP_2O_7)(NH_3)_2]^-\cdot NH_3$	−0.733	−0.763	−0.832	−0.866	−1.016 −0.983 (free NH_3)	1.427	1.447		1.044	0.399	0.374 0.347 (free NH_3)

Table 10 Selected normal vibrational wavenumbers (ν, stretching; δ, bending) in cm^{-1}. Intensities: w, weak; m, medium; s, strong; with the values in km mol^{-1}. The diagonal elements of the force constant matrix are in square brackets in mdyne $Å^{-1}$ or mdyne rad^{-1}

Molecule	ν[P–O(t)]	ν]P–O(b)]	ν(Cu–O)	δ[O(t)–P–O(t)]	δ(Cu–O–P)	δ(O–Cu–O)
$P_2O_7^{4-}$	912.5 m(558.6) [10.380]	721.5 s(1385.1) [5.738]		464.0 m(304.0) [2.429]		
		ν[P–O(b)]/ ν(Cu–O)	ν(Cu–O)/ ν[P–O(b)]			
$[Cu(P_2O_7)]^{2-}$	994.9 s(126.0) [11.890]	681.5 w(12.0) [4.727]	662.1 w(0.4) [4.954]	398.2 m(28.7) [1.831]	211.4 m(10.2) [0.545]	157.8 m(13.4) [0.431]

O(5B)–P(2B)–O(6B) angle [116.8(5)°], which is in front of O(6W), and the O(5A)–P(2A)–O(7A) angle [114.9(5)°], which is faced to O(2W2), are larger than the idealized tetrahedral value. Even though no linking interaction seems to exist on the basis of the O···P contact distances, this analysis suggests that a certain activation for nucleophilic attack by water on the phosphate groups of both the free and metal-bound nucleotide molecules occurs in this structure.

The protonation status of the nucleotides formulated as H_2ADP^- and ADP^{3-} for the free and metal-bound molecules, respectively, was inferred from the following series of observations. (1) The Fourier-difference map shows peaks on N(1B) and O(7B); no peaks were detected around N(1A) and O atoms from phosphate groups of the metal-bound nucleotide. (2) The P–O bond distances for the nucleotide molecules are consistent with protonation of the terminal phosphate of free nucleotide molecule only. (3) The values of the C(2)–N(1)–C(6) angles confirm the protonation of N(1B) only, on the basis of the Singh rule.[32] (4) A strong linkage of copper to a ligand molecule can increase significantly the acidity of the ligand protons especially in the portion of the molecule close to metal ligation. In this work the crystals were obtained from a mother-liquor composed of ethanol (*ca.* 50%) and water and no acid was added to increase the acidity. (5) Atoms N(1B) and O(3B) at $x,y+1,z$ have a contact distance of 2.66(2) Å [angle at H(N1B) 166(3)°] which is indicative of a hydrogen bond. It is not reasonable that an alpha-phosphate oxygen [like O(3B)] is protonated. So, only N(1B) can be a hydrogen donor, of the latter pair of atoms. In conclusion N(1B) is protonated. (6) Atoms O(7B) and O(2A) both at x,y,z have a contact distance of 2.65(1) Å [angle at H(O7B) 152(3)°] which is indicative of a possible hydrogen bond. Again, O(2A) is very reasonably not protonated; O(7B) is probably protonated.

All this evidence converges towards the formulation given in this work even though it is clear that each single observation alone is not strong enough to make the assumption reliable. A sound answer could come from a very accurate diffraction analysis carried out on larger single crystals possibly investi-

gated at low temperature and through a neutron beam. The authors recall that the best quality crystal used for the present data collection came after very many crystal growth attempts.

Finally, this work proves that density functional analysis, at least at the B3LYP/LANL2DZ level, is able to reproduce the copper(II)–pyrophosphate linkage and to give important physico-chemical parameters relevant to the copper(II)– and zinc(II)–nucleotide interactions. The positive charge on phosphorus atoms of phosphate and pyrophosphate ligands increases, even though slightly, upon co-ordination to copper(II). This effect and the computed distortion from the tetrahedral environment around phosphorus caused by the Cu^{II}–O(P) bond formation [for instance, the O(t)–P–O(t) angle for the computed $[Cu\{O(\alpha),O(\beta)\text{-}P_2O_7\}]^{2-}$ molecule is 120.7°) is in accord with the catalytic role copper(II) ions play in hydrolytic processes of nucleotides.

Acknowledgements

The authors thank Professor G. Sabatini, director, and Mr A. Scala for the collection of X-ray powder diffraction data at Istituto di Mineralogia e Petrografia, Università di Siena. Mr F. Berrettini, at Centro Interdipartimentale di Analisi e Determinazioni Strutturali, Università di Siena, is acknowledged for X-ray data collection. Università di Siena, Ministero dell′Università e della Ricerca Scientifica e Tecnologica (Roma), through grant COFIN.MURST 97-CIFSB, and Consiglio Nazionale delle Ricerche (Roma) are acknowledged for funding.

References

1 (*a*) K. Aoki, in *Metal Ions in Biological Systems*, eds. A. Sigel and H. Sigel, Marcel Dekker, Basel, 1996, vol. 32, ch. 4; (*b*) L. Stryer, *Biochemistry*, W. H. Freeman and Co., New York, 1991; (*c*) M. Ronaghi, M. Uhlén and P. Nyrén, *Science*, 1998, **281**, 363; (*d*) D. A. Suhy and T. V. O'Halloran, in *Metal Ions in Biological Systems*, eds. A. Sigel and H. Sigel, Marcel Dekker, Basel, 1996, vol. 32, ch. 16; (*e*) T. Steitz, S. J. Smerdon, J. Jäger and C. M. Joyce, *Science*, 1994, **266**, 2022; (*f*) J. P. Whitehead and S. J. Lippard, in *Metal Ions in Biological Systems*, eds. A. Sigel and H. Sigel, Marcel Dekker, Basel, 1996, vol. 32, ch. 20; (*g*) R. K. O. Sigel, E. Freisinger and B. Lippert, *Chem. Commun.*, 1998, 219; (*h*) M. Sabat, in *Metal Ions in Biological Systems*, eds. A. Sigel and H. Sigel, Marcel Dekker, Basel, 1996, vol. 32, ch. 15; (*i*) M. J. Bloemink, J. P. Dorenbos, R. J. Heetebrij, B. K. Keppler and J. Reedijk, *Inorg. Chem.*, 1994, **33**, 186; (*j*) N. Farrell, in *Metal Ions in Biological Systems*, eds. A. Sigel and H. Sigel, Marcel Dekker, Basel, 1996, vol. 32, ch. 18; (*k*) M. Coluccia, A. Nassi, F. Loseto, A. Boccarelli, M. A. Mariggio, D. Giordano, F. P. Intini and G. Natile, *J. Med. Chem.*, 1993, **36**, 510; (*l*) T. P. Kline, L. G. Marzilli, D. Live and G. Zon, *J. Am. Chem. Soc.*, 1989, **111**, 7057; (*m*) B. Song, A. Holý and H. Sigel, *Gazz. Chim. Ital.*, 1994, **124**, 387; (*n*) G. B. Helion, *Angew. Chem.*, 1989, **101**, 893.
2 J. Löwe and L. A. Amos, *Nature* (*London*), 1998, **391**, 203.
3 G. J. Davies, S. J. Gamblin, J. A. Littlechild, Z. Dauter, K. S. Wilson and H. C. Watson, *Acta Crystallogr. Sect. D*, 1994, **50**, 202.
4 S. Morera, I. Lascu, C. Dumas, G. LeBras, P. Briozzo, M. Véron and J. Janin, *Biochemistry*, 1994, **33**, 459.
5 J.-M. Lehn, *Supramolecular Chemistry; Concepts and Perspectives*, VCH, Weinheim, 1995.
6 J.-M. Lehn, *Science*, 1993, **260**, 1762.
7 S. H. Gellman (Guest editor), *Chem. Rev.*, 1997, 97.
8 L. J. Barbour, G. W. Orr and J. L. Atwood, *Nature* (*London*), 1998, **393**, 671.
9 J. C. Ma, D. A. Dougherty, *Chem. Rev.*, 1997, **97**, 1303.
10 A. Cavaglioni and R. Cini, *J. Chem. Soc.*, *Dalton Trans.*, 1997, 1149.
11 R. Cini, R. Bozzi, A. Karaulov, M. B. Hursthouse, A. M. Calafat and L. G. Marzilli, *J. Chem. Soc.*, *Chem. Commun.*, 1993, 889.
12 R. Cini, M. C. Burla, A. Nunzi, G. P. Polidori and P. F. Zanazzi, *J. Chem. Soc.*, *Dalton Trans.*, 1984, 2467.
13 P. Orioli, R. Cini, D. Donati and S. Mangani, *Nature* (*London*), 1980, **283**, 691.
14 R. Cini and R. Bozzi, *J. Inorg. Biochem.*, 1996, **61**, 109.
15 G. M. Sheldrick, SHELXS 86, Program for Crystal Structure Determination, University of Göttingen, 1986.
16 G. M. Sheldrick, SHELXL 93, Program for Refinement of Crystal Structure, University of Göttingen, 1993.
17 H. D. Flack, *Acta Crystallogr.*, *Sect. A*, 1983, **39**, 876.
18 M. Nardelli, PARST 95, A System of Computer Routines for Calculating Molecular Parameters from Results of Crystal Structure Analyses, University of Parma, 1995.
19 L. Zsolnai, ZORTEP, An Interactive ORTEP program, University of Heidelberg, 1994.
20 L. J. Farrugia, ORTEP 3 for Windows, Version 1.01 Beta, University of Glasgow, 1997.
21 M. J. Frisch, G. W. Trucks, H. B. Schlegel, P. M. W. Gill, B. G. Johnson, M. A. Robb, J. R. Cheeseman, T. Keith, G. A. Petersson, J. A. Montgomery, K. Raghavachari, M. A. Al-Laham, V. G. Zakrzewski, J. V. Ortiz, J. B. Foresman, J. Cioslowski, B. B. Stefanov, A. Nanayakkara, M. Challacombe, C. Y. Peng, P. Y. Ayala, W. Chen, M. W. Wong, J. L. Andres, E. S. Replogle, R. Gomperts, R. L. Martin, D. J. Fox, J. S. Binkley, D. J. Defrees, J. Baker, J. P. Stewart, M. Head-Gordon, C. Gonzalez and J. A. Pople, Gaussian Inc., Pittsburgh, PA, 1995.
22 A. D. Becke, *J. Chem. Phys.*, 1988, **88**, 1053; C. Lee, W. Yang and R. G. Parr, *Phys. Rev. B*, 1988, **37**, 785.
23 P. J. Hay and W. R. Wadt, *J. Chem. Phys.*, 1985, **82**, 299.
24 D. E. Woon and T. H. Dunning, Jr., *J. Chem. Phys.*, 1993, **98**, 1358 and refs. therein.
25 (*a*) H. Saint-Martin, L. E. Ruiz-Vicent, A. Ramírez-Solís and I. Ortega-Blake, *J. Am. Chem. Soc.*, 1996, **118**, 12167; (*b*) A. J. H Wachters, *J. Chem. Phys.*, 1970, **52**, 1033.
26 P. Swaminathan and M. Sundaralingam, *Acta Crystallogr.*, *Sect. B*, 1980, **36**, 2590.
27 Z. Shakked, M. A. Viswamitra and O. Kennard, *Biochemistry*, 1980, **19**, 2567.
28 M. Sabat, R. Cini, T. Haromy and M. Sundaralingam, *Biochemistry*, 1985, **24**, 7827.
29 W. Sanger, *Principles of Nucleic Acid Structure*, Springer, New York, 1984.
30 D. Cremer and J. A. Pople, *J. Am. Chem. Soc.*, 1975, **97**, 1354.
31 R. Cini, *Comments Inorg. Chem.*, 1992, **13**, 1.
32 C. Singh, *Acta Crystallogr.*, 1965, **19**, 861.
33 P. Prusiner and M. Sundaralingam, *Acta Crystallogr.*, *Sect. B*, 1972, **28**, 2148.
34 C. Altona and M. Sundaralingam, *J. Am. Chem. Soc.*, 1972, **94**, 8205.
35 O. Kennard, N. W. Isaacs, W. D. S. Motherwell, J. C. Coppola, D. L. Wampler, A. C. Larson and D. G. Watson, *Proc. R. Soc.*, *London*, *Ser. A*, 1971, **325**, 401.
36 J. V. Folgado, R. Ibáñez, E. Coronado, D. Beltrán, J. M. Savariault and J. Galy, *Inorg. Chem.*, 1988, **27**, 19.
37 M. C. Muñoz, R. Ruiz, M. Julve, F. Lloret and X. Solans, *Acta Crystallogr.*, *Sect. C*, 1993, **49**, 674.
38 R. Cini and L. G. Marzilli, *Inorg. Chem.*, 1988, **27**, 1855.
39 A. F. Wells, *Structural Inorganic Chemistry*, Clarendon Press, Oxford, 1975.
40 (*a*) D. Kobashi, S. Kohara, J. Yamakawa and A. Kawahara, *Acta Crystallogr.*, *Sect. C*, 1997, **53**, 1523; (*b*) R. Masse, J. C. Guitel and A. Durif, *Mater. Res. Bull.*, 1979, **14**, 337; (*c*) M. T. Averbuch-Pouchot and A. Durif, *Z. Kristallogr.*, 1987, **180**, 195.
41 R. Cini, D. G. Musaev, L. G. Marzilli and K. Morokuma, *J. Mol. Struct.* (*Theochem.*), 1997, **392**, 55.
42 B. Ma, C. Meredith and H. F. Schaefer III, *J. Phys. Chem.*, 1995, **99**, 3815.
43 H. Sigel and B. Song, in *Metal Ions in Biological Systems*, eds. A. Sigel and H. Sigel, Marcel Dekker, Basel, 1996, vol. 32 and refs. therein.
44 A. Bondi, *J. Phys. Chem.*, 1964, **68**, 441.

Paper 8/07793B